Nonlinear dynamics of a two-body nonlinear mechanical system

J. Awrejcewicz[1]

The University of Tokyo, Department of Mechanical Engineering, Hongo, Bunkyo-ku, Tokyo 113, Japan

Based on the example of a sixth-order set of nonlinear differential equations governing the dynamics of a mechanical system with three degrees of freedom, this paper presents a numerical method for the systematic tracing of structural changes of the phase flow, which accompanies changes in the chosen system parameters. The periodic orbits are traced by solving a boundary problem with the shooting and Newton–Raphson methods. Irregular motions are observed using the standard methods based on the solution of the initial value problem. Two different scenarios leading to chaos, as well as some special examples of chaotic dynamics, are discussed and illustrated.

1. Introduction

Nonlinear differential equations of motion governing the dynamics of complex mechanical systems are often solved numerically. The reason as widely described in the literature is that approximate analytical methods are generally available only for weak nonlinearities and for oscillations with small amplitudes [1–10]. They allow only for a local investigation of the nonlinear dynamics of the considered system. Additionally, if the nonlinear dynamics changes qualitatively (after bifurcation), another analytical approach should be used to analyze the behavior of the system in this new dynamical state. If analytical asymptotic techniques, such as the method of averaging or the method of multiple time scales are applied, their range of applicability must be considered. Without an estimation of the small parameter (the parameter of the asymptotic analysis) for which the solution of the averaged equations has quantitative and qualitative correspondence with the exact solutions of the original system, the results obtained can be wrong. On the other hand, such an analysis is complicated, and only in a few cases has it been carried out [11–15].

For these reasons, complex mechanical nonlinear systems which include nonlinearities often have to be investigated by numerical methods. These methods are based on the general theorems concerned with nonlinear dynamics [16–19] and allow a systematical study of the global nonlinear behavior of multi-body mechanical systems.

For engineering purposes it is particularly important to know the changes of the phase flow

[1] On leave from Technical University, Institute of Applied Mechanics, B. Stefanowskiego 1/15, 90-924 Lodz, Poland.

of the analyzed dynamical system in a certain space of parameter changes. The presented numerical approach not only allows this possibility, but permits the determination of the critical (bifurcation) parameter set which separates the qualitatively different behaviors of the system (i.e., periodic, quasiperiodic and chaotic motion).

Periodic orbits are traced, with the change of a freely chosen control parameter, by solving a boundary value problem. Use of the Newton–Raphson procedure, as well as the shooting method, has made it possible to trace the periodic orbit changes accompanying the changes in the control parameter with a simultaneous tracing of the multipliers' values. The latter are crucial for the stability and bifurcation of the considered periodic orbits. A similar method, based on the Urabe [20, 21] procedure, has been successfully applied to the computation of bifurcation points and periodic orbits of the rotor vibrations studied earlier by Brommundt [22, 23]. A similar strategy has also been presented by Seydel [24].

The calculation method used here also allows for accurate determination of the bifurcation points, which in the case of the saddle-node bifurcation can lead to finding the critical parameters and, after passing them, chaos appears.

The chaotic behavior is traced using the standard methods based on the solution of the initial value problem (time histories, attractors projections' on the phase planes or Poincaré map projections).

In this paper, such a numerical technique is applied to the study of a rotor having different cross-section moments and nonlinearly supported in a rigid, sinusoidally-excited frame. Two different scenarios leading to chaos are discussed and demonstrated. Additionally, if the dimensionless coefficient b equals zero (the coefficient being proportional to the parametric amplification), the motions of the rotor and of the frame are independent. An increase in b, however, couples both the motions. This makes it possible to analyze the following important question: In what way can two different attractors, a regular and an irregular one, interact with an increase in a control parameter?

The above calculation strategy has been used by the author in nonlinear analyses of simple [25, 26] and coupled oscillators [27, 28].

2. The analyzed system and equations of motion

A diagram of the analyzed system is presented in Fig. 1 (a system very similar to this was earlier considered in [29]). A weightless rotor, with a rectangular cross-section, is fixed in the rigid bearings of a rigid frame. The frame, which only moves horizontally, is supported in a nonlinear fashion. Also, the cylindrical mass m, concentrated in the middle of the rotor, is nonlinearly supported in the x_2 direction.

The theoretical model of the analyzed rotor is presented in Fig. 1(b). The equations of motion of the rotor have the form

$$m\ddot{x}_c = -\xi_\omega k_\xi \cos\phi - \eta_\omega k_\eta \sin\phi , \qquad m\ddot{y}_c = \xi_\omega k_\xi \sin\phi - \eta_\omega k_\eta \cos\phi + mg ,$$

$$I_z\ddot{\phi} = -M_0 + \alpha(-\xi_\omega k_\xi \cos\phi_0 + \eta_\omega k_\eta \sin\phi_0) , \tag{1}$$

where x_c, y_c are the coordinates of the center of mass of the cylinder, I_z is the mass moment of
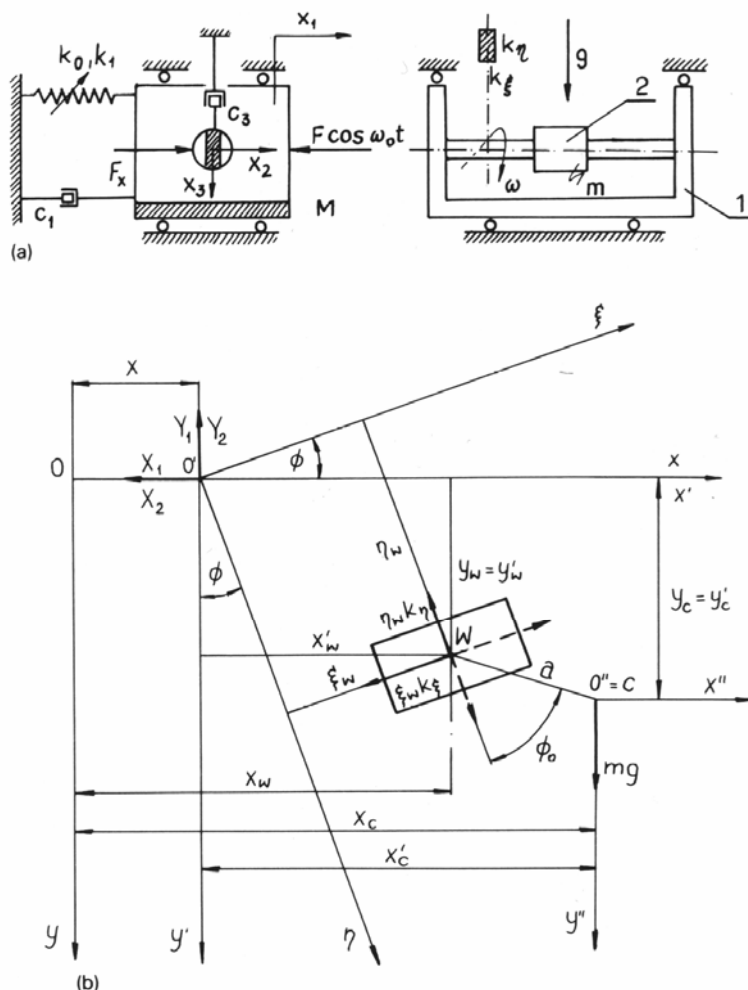
Fig. 1. The analyzed system (a) and a theoretical diagram of the rotor (b).

inertia of a cylinder mass m, in relation to the z axis, ξ_ω, η_ω are the coordinates of the point of puncture by the rotor in the coordinate system, $O'\xi\eta$ is the coordinate system whose axes are parallel to the main, central, inertial axes of the rotor cross section, k_ξ, k_η are the rotor rigidities in the direction of the axes ξ and η, M_0 is the driving torque reduced by all the resistance torques, and α, ϕ_0 are the parameters characterizing the position of the center of mass of the disk C in relation to the point of puncture of the rotor. For states near steady state, the torque M_0 is very small. Let I_z be represented by

$$I_z = mi_s^2 , \tag{2}$$

where i_s is the inertia radius. The third equation of (1) then assumes the form

$$\ddot{\phi} = (\alpha/mi_s^2)(-\xi_\omega k_\xi \cos \phi_0 + \eta_\omega k_\eta \sin \phi_0) . \tag{3}$$

Since the eccentricity a and the rotor deflections ξ_ω and η_ω are small compared to the inertia

radius, we obtain

$$\ddot{\phi} = 0 , \qquad \dot{\phi} = \omega = \text{const} , \qquad \phi = \omega t . \tag{4}$$

The following geometric dependences result from Fig. 1(b):

$$\xi_\omega = (x_\omega - x) \cos \phi - y_\omega \sin \phi , \qquad \eta_\omega = (x_\omega - x) \sin \phi - y_\omega \cos \phi ,$$

$$y_c = y_\omega + \alpha \cos(\phi + \phi_0) , \qquad x_c = x_\omega + \alpha \sin(\phi + \phi_0) , \tag{5}$$

where x_ω, y_ω are the coordinates of the point of puncture by the rotor W in the system Oxy.

In order to write down the equations of motion for the mass M, it is first necessary to determine dynamic reactions on the rotor at its points of support. They are obtained from the equations

$$X_1 + X_2 + \xi_\omega k_\xi \cos \omega t + \eta_\omega k_\eta \sin \omega t = 0 ,$$

$$Y_1 + Y_2 - \xi_\omega k_\xi \sin \omega t + \eta_\omega k_\eta \cos \omega t = 0 , \tag{6}$$

where X_1, Y_1 and X_2, Y_2 denote the support reactions on the left and right ends of the rotor, respectively.

After assuming that $x = x_1$, $x_\omega = x_2$, $y_\omega = x_3$ and additionally that the force $F_x = k_\alpha x_2$ is acting on the mass m in the x_2 direction, the following governing equations are obtained:

$$M\ddot{x}_1 + c_1\dot{x}_1 - k_0 x_1 + k_1 x_1^3 + (\tfrac{1}{2}(k_\xi + k_\eta) + \tfrac{1}{2}(k_\xi - k_\eta) \cos 2\omega t)x_1$$

$$- (\tfrac{1}{2}(k_\xi + k_\eta) + \tfrac{1}{2}(k_\xi - k_\eta) \cos 2\omega t)x_2 + \tfrac{1}{2}(k_\xi - k_\eta)x_3 \sin 2\omega t = F \cos \omega_0 t ,$$

$$m\ddot{x}_2 + c_2\dot{x}_2 - (\tfrac{1}{2}(k_\xi + k_\eta) + \tfrac{1}{2}(k_\xi - k_\eta) \cos 2\omega t)x_1$$

$$+ (\tfrac{1}{2}(k_\xi + k_\eta) + \tfrac{1}{2}(k_\xi - k_\eta) \cos 2\omega t)x_2 - k_\alpha x_2 - \tfrac{1}{2}(k_\xi - k_\eta)x_3 \sin 2\omega t$$

$$= m\alpha\omega^2 \sin(\omega t + \phi_0) , \tag{7}$$

$$m\ddot{x}_3 + c_3\dot{x}_3 + \tfrac{1}{2}(k_\xi - k_\eta)x_1 \sin 2\omega t - \tfrac{1}{2}(k_\xi - k_\eta)x_2 \sin 2\omega t$$

$$+ (\tfrac{1}{2}(k_\xi + k_\eta) - \tfrac{1}{2}(k_\xi - k_\eta) \cos 2\omega t)x_3$$

$$= m\alpha\omega^2 \cos(\omega t + \phi_0) + mg ,$$

$$k_\alpha = (\tfrac{1}{2}(k_\xi + k_\eta) + \tfrac{1}{2}(k_\xi - k_\eta) \cos 2\omega t) - k_2 \chi_2^2 ,$$

where x_1 is the horizontal displacement of the base; x_2 and x_3 are the horizontal and vertical displacement of the concentrated mass m situated in the middle of the rotor length; M is the base mass; k_0 and k_1 are the stiffnesses connecting the base with a motionless system; ω is the frequency of the rotor revolutions; F and ω_0 are the amplitude and the frequency of the

external forcing; c_1, c_2 and c_3 denote the viscous damping; g is the acceleration due to gravitation; k_2 the Duffing-type stiffness and r the amplification coefficient. The force F_x can be applied, for example, by induction of an automatic control. Examples of chaotic behavior in systems with a Duffing-type stiffness of the form $-k_0 x_1 + k_1 x_1^3$ are considered in a book by Thompson and Stewart [30]. From the relations given below,

$$\tau = (k_0 M^{-1})^{1/2} t, \qquad y_1 = (k_1 k_0^{-1})^{1/2} x_1, \qquad x_2 = \frac{2mgy_3}{k_\xi + k_\eta}, \qquad x_3 = \frac{2mgy_5}{k_\xi + k_\eta},$$

$$z = \frac{k_\xi + k_\eta}{2}, \qquad b = \frac{k_\xi - k_\eta}{2k_0}, \qquad d_1 = c_1 (k_0 M)^{-1/2}, \qquad e = mg(k_1 k_0^{-3})^{1/2},$$

$$\nu = \omega (M k_0^{-1})^{1/2}, \qquad \mu = mM^{-1}, \qquad q = F(k_1 k_0^{-3})^{1/2}, \qquad \nu_0 = \omega_0 (M k_0^{-1})^{1/2},$$

$$q_1 = \omega^2 \alpha g^{-1} \cos \phi_0, \qquad q_2 = \omega^2 \alpha g^{-1} \sin \phi_0, \qquad d_2 = \frac{2c_2 (k_0 M^{-1})^{1/2}}{(k_\xi + k_\eta)},$$ (8)

$$d_3 = \frac{2c_3 (k_0 M^{-1})^{1/2}}{(k_\xi + k_\eta)}, \qquad \gamma = 8k_2 m^2 g^2 (k_\xi + k_\eta)^{-3}, \qquad \frac{\mathrm{d}}{\mathrm{d}\tau} = {}',$$

$$\varepsilon = \frac{b}{z} = \frac{k_\xi - k_\eta}{k_\xi + k_\eta},$$

the following nondimensional set of equations is obtained:

$$y_1' = y_2,$$

$$y_2' = (1 - z)y_1 - y_1^3 - by_1 \cos 2\nu\tau - d_1 y_2 + ey_3(1 + \varepsilon \cos 2\nu\tau)$$
$$\qquad - \varepsilon ey_5 \sin 2\nu\tau + q \cos \nu_0 \tau,$$

$$y_3' = y_4,$$

$$y_4' = \frac{z}{\mu}\left\{ \frac{z}{e} y_1(1 + \varepsilon \cos 2\nu\tau) + ry_3(1 + \varepsilon \cos 2\nu\tau) \right.$$ (9)

$$\qquad \left. + \varepsilon y_5 \sin 2\nu\tau - d_2 y_4 - \gamma y_3^3 + q_1 \sin \nu\tau + q_2 \cos \nu\tau \right\},$$

$$y_5' = y_6,$$

$$y_6' = \frac{z}{\mu}\left\{ -\frac{z}{e} \varepsilon y_1 \sin 2\nu\tau + \varepsilon y_3 \sin 2\nu\tau - y_5(1 - \varepsilon \cos 2\nu\tau) \right.$$

$$\qquad \left. - d_3 y_6 + 1.0 + q_1 \cos \nu\tau + q_2 \sin \nu\tau \right\}.$$

3. The method

The periodic orbits of the equation system (9) have been traced by solving the boundary-value problem. The integration of the differential equations has been performed using the Gear method [31]. The idea behind this method consists of the construction of the mapping $M(y^{(k)}) = M^{(k)}$, while the distance between two arbitrary consecutive points in the case of nonautonomous systems analysis is equal to the period of the sought solution. The error $E = y^{(k)} - M^{(k)}$ gauges the accuracy of the estimation (k). Thanks to the shooting method and the Newton–Raphson procedure, we can look for the values of E. The calculations are interrupted if $\|E\| = |E| \leqslant 10^{-5}$.

The stability analysis of the calculated periodic solutions is reduced to an analysis of the linear differential equation systems having the periodic coefficients

$$\Delta p' = J(\tau)\,\Delta p = (\partial y'/\partial y)_{y_p(\tau)}\,\Delta p\,, \tag{10}$$

where $J(\tau + T) = J(\tau)$ and Δp is a perturbation vector of the investigated periodic solution $y_p(\tau)$.

According to the Floquet theory, the general solution of (10) is

$$\Delta p = \Phi(\tau)\,\Delta p(0)\,, \tag{11}$$

where $\Phi(\tau) = \Phi(\tau + T)$ is the fundamental matrix. The eigenvalues of the matrix $\Phi(T) = \partial M/\partial y$, which are the multipliers, are known from the iteration mentioned above as the Jacobi matrix of the point mapping at the fixed point.

The multipliers determine the stability and bifurcation of the considered periodic orbit. In the case where one of the multipliers is real and crosses the unit circle of the complex plane at the point -1 from the direction outside the circle, the considered periodic orbit becomes unstable. A new orbit, with a period two times greater, branches from it.

In the case where the transition conditions given above are retained, if one of the multipliers exceeds the value of $+1$, the considered periodic orbit becomes unstable, and either an orbit with one half of its former period, or a chaotic orbit appears.

The last of the classical cases occurs when a pair of complex conjugate characteristic multipliers crosses the unit circle of the complex plane. In this case a new periodic, or quasiperiodic, solution can appear [32].

In order to examine the chaotic behavior of the analyzed system, a Poincaré map associated with (9) is used. This map has been defined as the following sectional surface:

$$\sum_{t_0}^{t_n} = \{\{y_i(t_n),\, y_j(t_n)\}\,, \quad t_n = t_0 + 2\pi n \nu_0^{-1}\}\,.$$

4. Two different routes to chaos

The numerical method described in the previous section has been applied to trace the scenarios leading to chaos in our system. Calculations have been made for the following

constant parameters: $z = e = d_1 = \mu = 0.1$, $\nu = \nu_0 = 0.7$, $q = q_2 = 0.0$, $q_1 = 1.0$, $r = \gamma = 0.5$ and $d_2 = d_3 = 0.01$. On the basis of the boundary problem solution, the changes in two periodic orbits found on the left and right side of the origin, which accompanied the changes in b, were traced. For $b = 10^{-5}$ a constant point of Poincare's map has been found ($y_1 = 0.6993$, $y_2 = 0.16294$, $\dot{y}_3 = 0.28719$, $y_4 = 1.1982$, $y_5 = 2.8236$ and $y_6 = 0.35041$). The eigenvalues of the Floquet matrix corresponding to that point are $(0.59 \pm 0.13i)$, $(-0.26 \pm 0.35i)$ and $(-0.36 \pm 0.19i)$. The orbit has been further traced with the increase in b to the value 0.0407. Within the range of $b \in \{10^{-5}, 0.0378\}$, the orbit is stable (Fig. 2(a)). For $b = 0.040609$, it becomes stable again, while for $b = 0.040701$ a saddle-node bifurcation occurs. After passing the latter value of b, chaos appears, with its projection $y_3(y_2)$ for $b = 0.042$ corresponding to the mass m trajectory shown in Fig. 2(c). As an example Fig. 2(c) gives, for $b = 0.038$, the time histories of the unstable periodic orbit.

Similarly, the periodic orbit found on the left side of the coordinate system has been traced. The solution branch y_1 is shown in Fig. 2(d) (the starting point for $b = 10^{-5}$ is $y_1 = -1.0689$, $y_2 = -0.0474$, $y_3 = -5.8$, $y_4 = -0.346$, $y_5 = 1.0$ and $y_6 = 5.0$). The traced periodic orbit is stable to the point Q ($b = 0.0097$). From that point branches the quasiperiodic solution, which loses its stability after a slight increase in b and chaos appears. Figure 2(e) displays the time courses of the observed solution at the critical point Q, while in Fig. 2(f) the projection of the strange chaotic attractor $y_3(y_2)$, for $b = 0.012$, is shown.

It is worth stressing that the former of the traced orbits has the period $T = 2\pi/\nu_0$, while the second one has the period $2T/3$. The former disappears due to the saddle-node bifurcation and a chaotic orbit appears. In the second case, after a bifurcation a quasiperiodic solution appears which exists within a very narrow range of b, and a strange chaotic attractor is born in its place.

5. Observation of chaotic dynamics

Numerical calculations have been made for the following parameters: $z = d_1 = d_2 = d_3 = \mu = 0.1$, $\nu = 0.8$, $\nu_0 = 1.0$, $q_1 = 0.15$, $q_2 = 0.0$, $E = 0.01$ and $r = \gamma = 0.5$. If $b = 0$, then $\varepsilon = 0$ as well. This means that the oscillations of $y_5(\tau)$ are regular. Chaotic oscillations of the concentrated mass m are presented in Fig. 3, which contains the Poincaré map projections $y_1(y_1')$ and $y_2(y_2')$. With an increase in b, the chaotic dynamics of the rotor also increases, and chaotic oscillations are transferred onto the coordinate $y_5(\tau)$. This is illustrated by Fig. 4, where the Poincaré map is projected to the three chosen planes in a similar way as before. If the projections presented in Fig. 4(a,b) indicate the strangeness of the analyzed attractor, it is clearly seen that the projection $y_3(y_3')$ consists of points placed on sections of lines arranged radially. It is a result of the compromise between the oscillations of the linear subsystem (rotor) in the y_3 direction, and the chaotic motions $y_1(\tau)$ and $y_2(\tau)$ coupled through b. The coupling increases with an increase in b. A certain hierarchy of chaotic motions can be noticed here. The travel of phase trajectories in the direction to the left and to the right of the origin of the coordinate system is several times faster for $y_1(\tau)$ than for $y_2(\tau)$. The time history $y_3(\tau)$ consists of intervals of regular motions, either increasing or decreasing in time, with evident jumps between those intervals. The motion shows, however, a certain characteristic order, which is illustrated on the projection of the $y_3'(y_3)$ map.
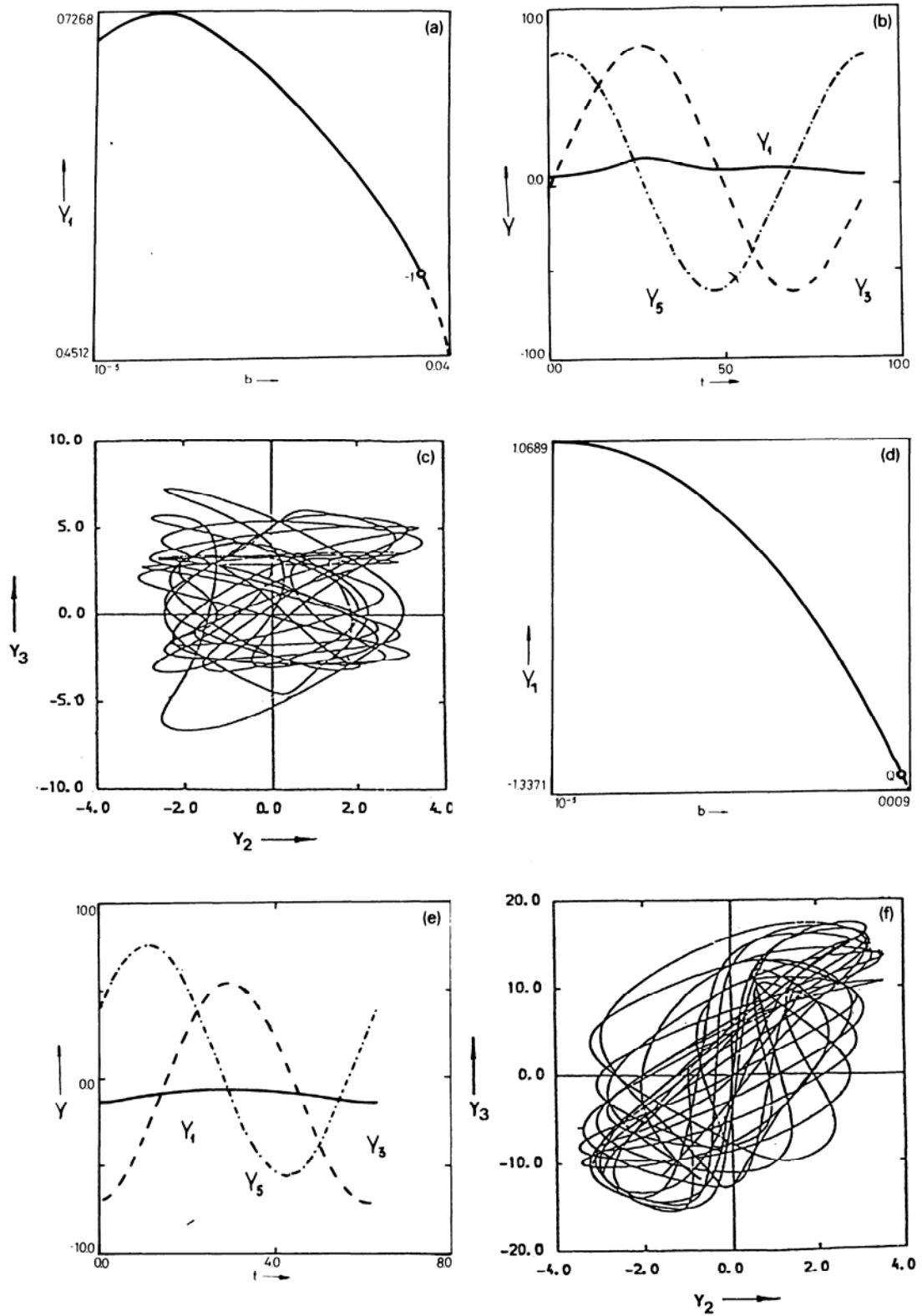
Fig. 2. Branches of the solution y_1 versus b, time courses, and the strange attractors projections to the left (a, b, c) and to the right (d, e, f) of the coordinate system origin.
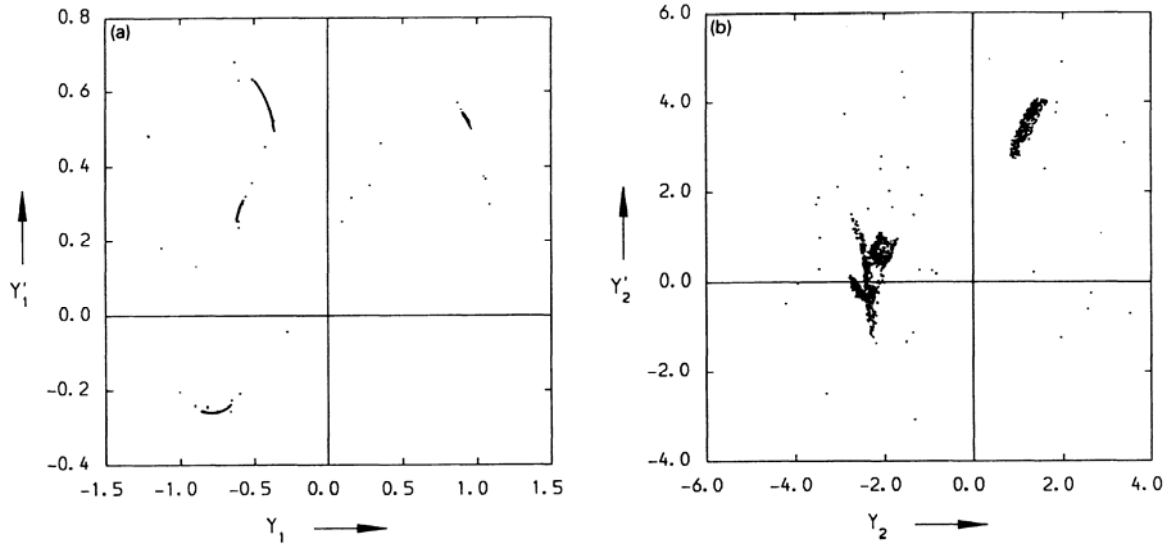
Fig. 3. Projections of a chaotic attractor (Poincaré map) onto (a) the (y'_1, y_1) and (b) (y'_2, y_2) planes ($E = 0.01$, $\mu = 0.1$, $b = 10^{-5}$).

In a way similar to that described above, the evolution of chaotic attractors accompanying the changes in b for $E = 0.1$ and $E = 1.0$ is carried out (the other parameters are the same as in the previous case).

In the case of $E = 0.1$, the chaotic dynamics are much greater as compared with the case considered earlier ($E = 0.01$). For example, the projection $y'_3(y_3)$ of the chaotic attractor (Poincaré map) presented for $b = 0.05$ in Fig. 5 does not show the characteristic regularity, which has been clearly seen for $b = 0.08$ and $E = 0.01$ (Fig. 4(c)). For $E = 1.0$ and during
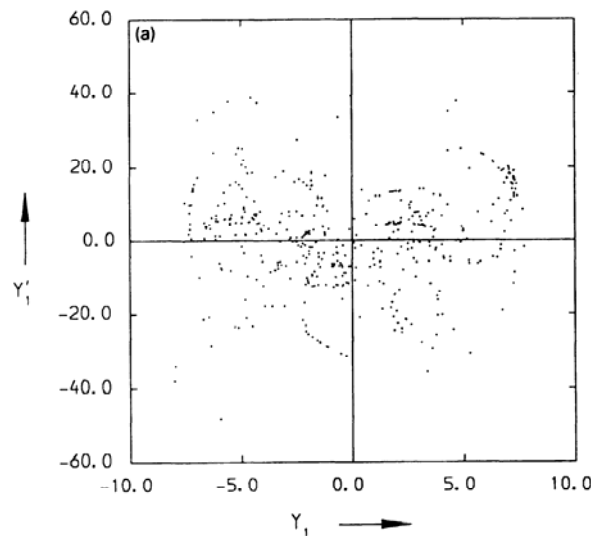
Fig. 4. Projections of a chaotic attractor (Poincaré map) onto the $(y'_1, y_1 : a)$, $(y'_2, y_2 : b)$ and $(y'_3, y_3 : c)$ planes for $E = 0.01$, $\mu = 0.1$, $b = 0.08$.
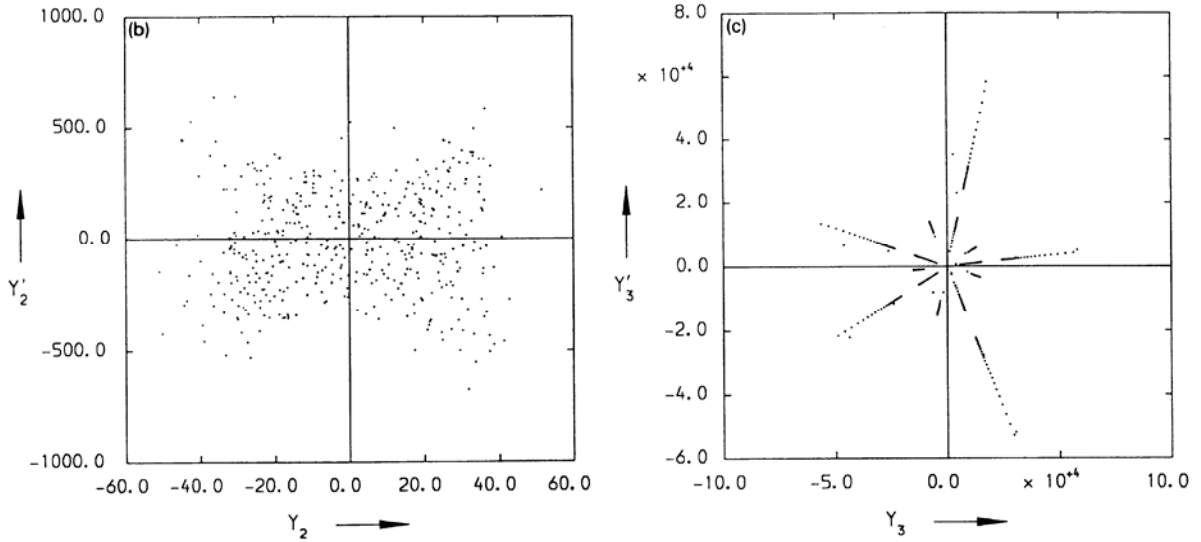
Fig. 4 (Continued).

changes in b within the range $[0.0, 0.08]$ certain qualitatively new behaviors of the analyzed system have been found. Similarly to the examples given above, the chaotic dynamics of the orbits increase with an increase in b. Typical time histories (Fig. 6) and three projections of Poincare maps (Fig. 7) are shown for $b = 0.05$. As can be seen from Fig. 7(c), the points of the map are irregularly arranged and are concentrated in five isolated islands. A further increase in b, as opposed to the earlier examples, brings about an increase in the ordering of the points, which are arranged along the radially placed sections of lines (Fig. 8).
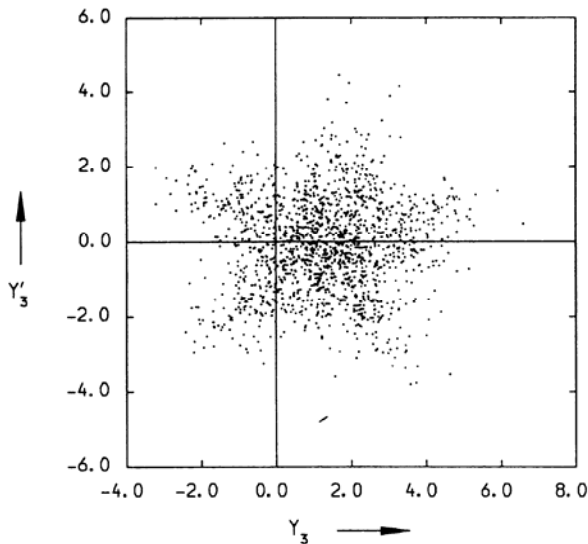

Fig. 5. Poincaré map projection $y_3'(y_3)$ of a strange chaotic attractor ($E = 0.1$, $b = 0.05$).
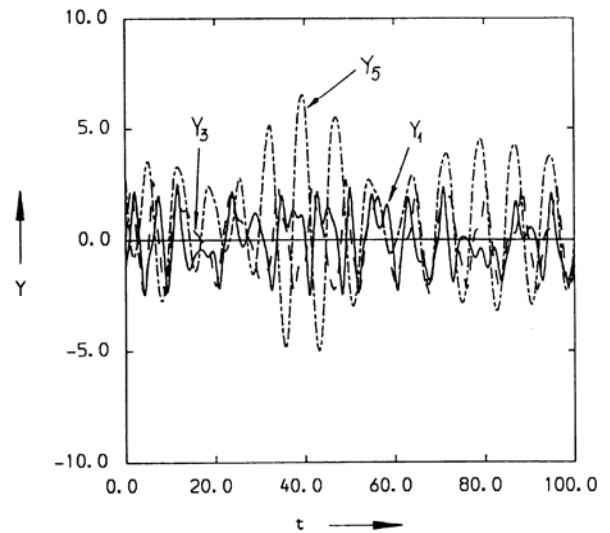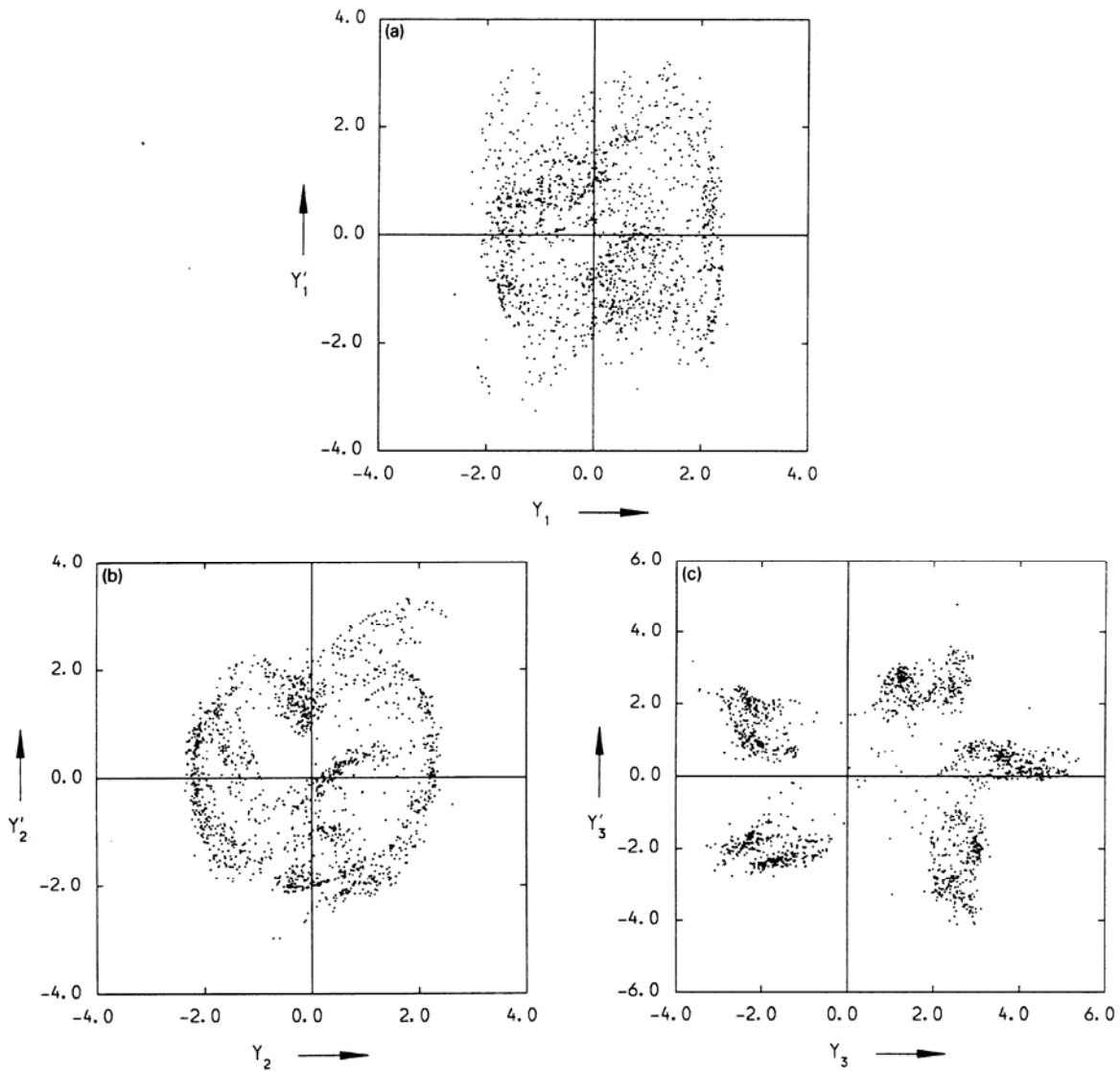
Fig. 6. Chaotic attractor for $E = 1.0$, $b = 0.05$.

Fig. 7. Three projections of a strange chaotic attractor ($E = 1.0$, $b = 0.05$).

A particular kind of order in the arrangement of the Poincaré map points has also been found for another parameter set. The parameters used for the calculation are the same as before, and $\mu = 10.0$. For $b = 10^{-5}$, three attractor projections are shown in Fig. 9. A characteristic order in the arrangement of the map points can be seen in the projections of $y_2'(y_2)$ and $y_3'(y_3)$. The increase in b disturbs the structure of that attractor, and it is replaced by a new one with projections shown in Fig. 10. The projections $y_2'(y_2)$ and $y_3'(y_3)$ shown in this figure make it possible to draw certain conclusions concerning the system dynamics. The phase curve $y_2'(y_2)$ travels between the points -1 and $+1$, and it is very strongly repelled near the former point, while being very strongly attracted near the point $+1$ (Fig. 10(a)).

As distinguished from the motion of the trajectory $y_2(\tau)$, the trajectory $y_3(\tau)$ moves only around the point $+1$, while the points of the map form a characteristic structure (Fig. 10(b)).
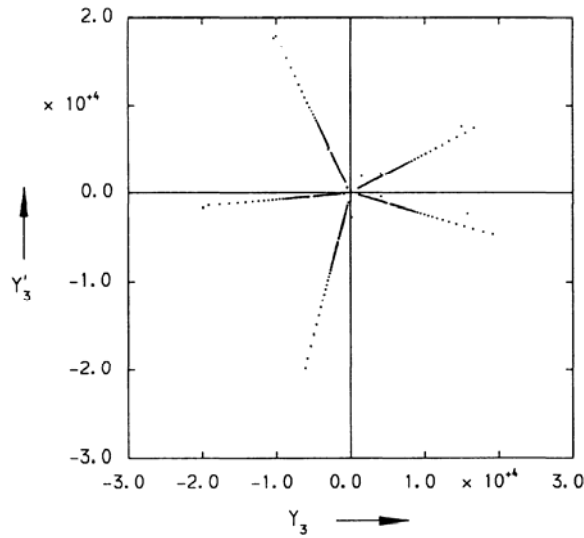
Fig. 8. Poincaré map projection $y_3'(y_3)$ ($E = 1.0$, $b = 0.08$).

A certain analogy to the results obtained by Neimark [33] is brought to mind here. He analyzed a simple dynamical system governed by the equations

$$\dot{\psi} = \frac{\partial H}{\partial r} + \nu H \frac{\partial H}{\partial \psi} + \mu f(\psi, r, t) \,, \qquad \dot{r} = -\frac{\partial H}{\partial \psi} + \nu H \frac{\partial H}{\partial r} + \mu g(\psi, r, t) \,, \qquad (12)$$

where $H = r^2 + \lambda \sin q\psi - \lambda$ (q is integer, $\lambda > 0$) and f and g are periodic functions with period 2π. The phase curves were governed by the equation $H(\psi, r) = r^2 + \lambda \sin q\psi - \lambda = $ const, and for $H = 0$ curves dividing the regions of $H > 0$ and $H < 0$ were obtained. The curves connected several saddles in a closed system. An increase in the parameter μ
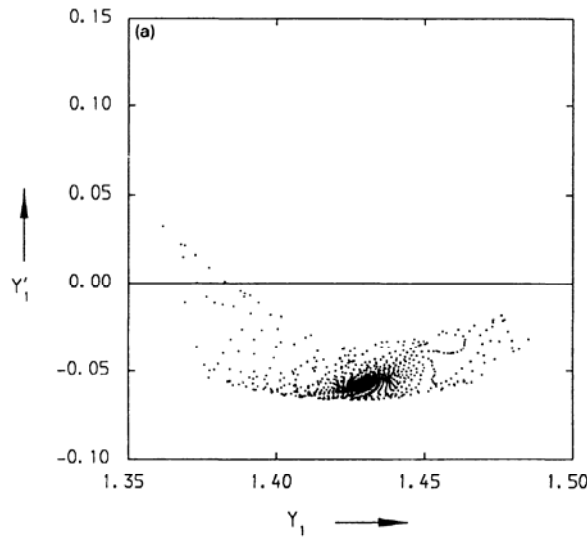
Fig. 9. Three Poincaré map projections of an attractor found for $E = \mu = 10.0$, $b = 0.05$.
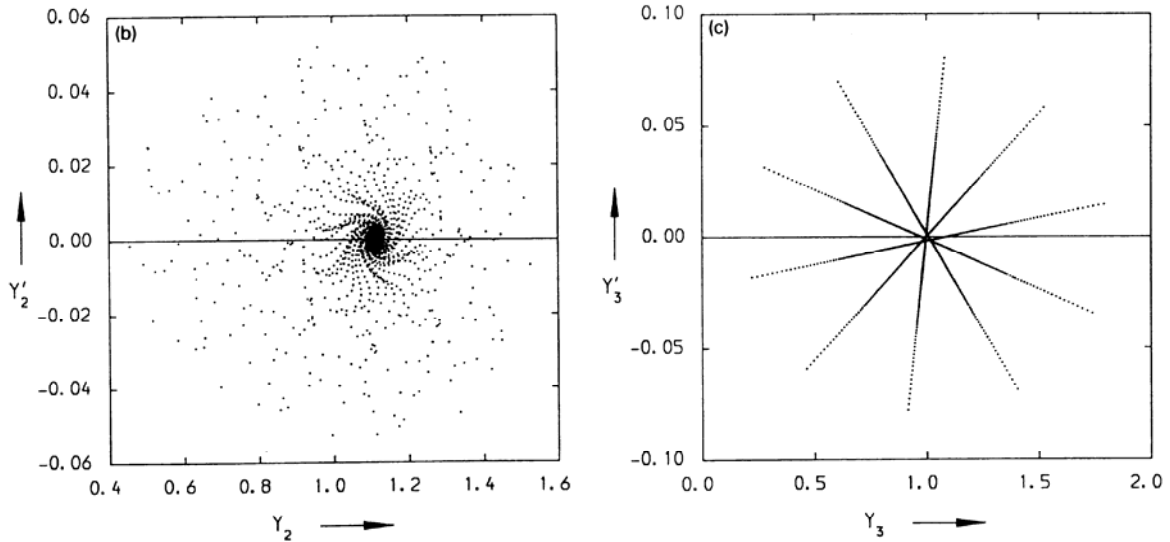
Fig. 9 (Continued).

corresponds to the turn of the field, and at a certain critical value a homoclinic structure is found around each of the saddles. Near such structures, transition to the neighboring homoclinic structures is incidental. Thence, despite a characteristic symmetry of the attractor, the motion observed is a chaotic one.

A further increase in the parameter b causes a diminishing of the attraction of point $+1$ until it attains a negative value. Finally, both points repel the trajectories, and they create an attractor which is approximately symmetrical about the horizontal and vertical axes crossing point $(0,0)$ (Fig. 11).
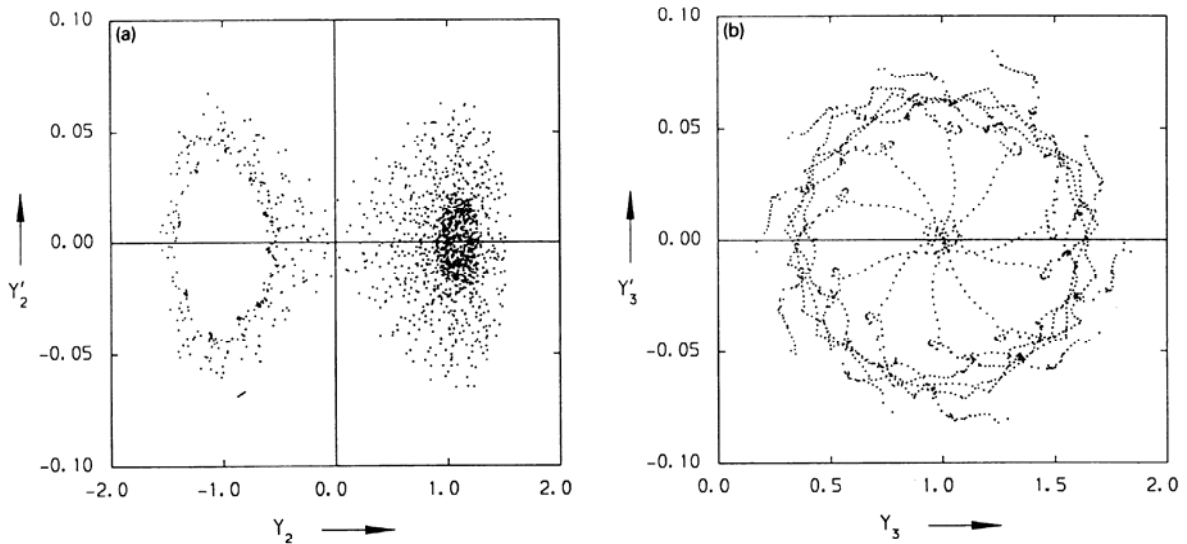

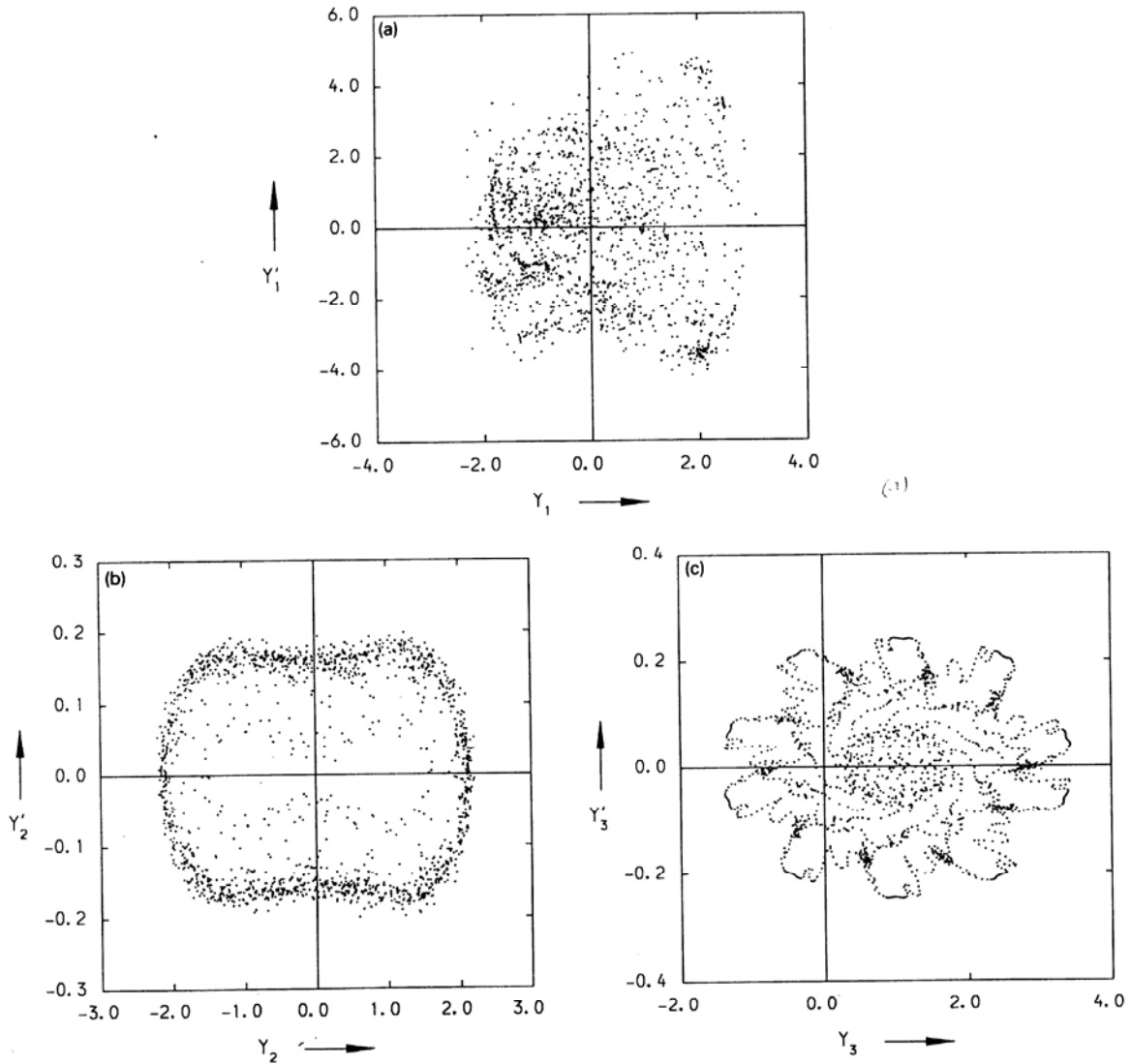Fig. 10. Two projections of a strange attractor ($E = \mu = 10.0$, $b = 0.05$).

Fig. 11. Three projections of a strange attractor for $E = \mu = 10.0$, $b = 0.08$.

6. Concluding remarks

This paper presents a general numerical strategy to analyze the regular and irregular dynamics of complex nonlinear mechanical systems. As an example, a two-body nonlinear mechanical system, containing a rotor with a rectangular cross-section is considered. This system is governed by ordinary sixth-order nonlinear differential equations with periodic coefficients. Two fundamental calculation examples are carried out. In the first example, a transition from regular to irregular motion (by solving both a boundary and an initial value problem) are discussed and illustrated. Results obtained in the second example are based on the solution of the initial value problem.

On the basis of the presented calculation analysis, it has been shown that in complex dynamical systems, the chaotic dynamics can differ considerably from that found in simple three-dimensional ones. The most important results are briefly summarized below:

1. Observation of periodic orbits (found on the left and the right side of the origin) based on solving a boundary value problem demonstrate different shift routes to chaos. The traced left periodic orbit is stable to the point Q, where a quasiperiodic attractor appears. A further slight increase in b causes another bifurcation, and a strange chaotic attractor is born. The right periodic orbit has disappeared due to the saddle-node bifurcation, and chaos appears. Additionally, the right periodic orbit has the period $T = 2\pi/\nu_0$, while the second has the period $2T/3$.

2. The rotor motion in the direction y_3 is coupled with the other two coordinates via the coefficient b proportional to the parametric excitation. For $b = 0$, the oscillations of $y_3(\tau)$ are linear, and through an increase in b it is possible to trace the interaction between the regular and the chaotic attractor (the parameters are chosen in such a way, that the oscillations $y_1(\tau)$ and $y_2(\tau)$ are chaotic). As a result of compromise between the two attractors, it is possible to observe on the Poincaré projection $y_3'(y_3)$ (for several parameter sets) a certain specific system of points, forming sections radiating out from the coordinate system origin.

3. Generally, in all the analyzed cases, an increase in b caused an increase in chaotic dynamics. This can be explained by the fact that with an increase in b, the parametric unstability zone grows, which causes an increase in the exponential divergence of the observed orbits.

4. Particularly interesting dynamics are illustrated in Figs. 10 and 11. The phase curve $y_2'(y_2)$ is strongly repelled near the point -1 (no points are noticeable in the Poincaré map projection), while it is strongly attracted near the point $+1$. Its travel between these points is unpredictable (chaotic). The trajectory $y_3(\tau)$ moves only around the point $+1$, while the points of the map form a characteristic symmetrical system, with several homoclinic structures.

References

[1] I.G. Malkin, Some Problems in the Theory of Nonlinear Oscillation (Nauka, Moscow, 1956) in Russian.
[2] N.N. Bogoliubov and Y.A. Mitropolskii, Asymptotic Methods in the Theory of Nonlinear Osillations (Hindustan Publishing Corp., Delhi, 1961).
[3] I.G. Malkin, Stability Theory of Motion (Nauka, Moscow, 1968) in Russian.
[4] N.G. Cetaiev, Stability of Motion (Nauka, Moscow, 1965) in Russian.
[5] D.R. Merkin, Introduction to the Stability of Motion Theory (Nauka, Moscow, 1976) in Russian.
[6] B.P. Demidovic, Mathematical Theory of Stability (Nauka, Moscow, 1967).
[7] G.E. Giacaglia, Perturbation Methods in Non-Linear Systems (Springer, New York, 1972).
[8] V.A. Iakubovic and V.M. Starzhinskii, Linear Differential Equations with Periodic Coefficients and Their Application (Nauka, Moscow, 1972) in Russian.
[9] A.H. Nayfeh and D.T. Mook, Nonlinear Oscillations (Wiley/Interscience, New York, 1979).
[10] A.H. Nayfeh, Introduction of Perturbation Techniques (Wiley/Interscience, New York, 1981).
[11] V.I. Zubov, Theory of Oscillations (High School, Moscow, 1979) in Russian.
[12] W.P. Rubanik, Oscillations in Complex Quasilinear Systems with Delay (University Press, Minsk, 1985) in Russian.

[13] A.M. Samoilenko, Elements of the Mathematical Theory of Multifrequency Oscillations. Invariant Orbits (Nauka, Moscow, 1987).

[14] S.M. Shapiro and P.R. Sethna, An estimate for the small parameter in the asymptotic analysis of non-linear systems by the method of averaging, Internat. J. Non-Linear Mech. 12 (1977) 127–136.

[15] A.K. Bajaj and J.M. Johnson, Asymptotic techniques and complex dynamics in weakly non-linear forced mechanical systems, Internat. J. Non-Linear Mech. 25 (2/3) (1990) 211–226.

[16] J.K. Hale, Ordinary Differential Equations (Wiley/Interscience, New York, 1969).

[17] P. Hartman, Ordinary Differential Equations (Wiley, New York, 1964).

[18] S.-N. Chow and J.K. Hale, Methods of Bifurcation Theory (Springer, New York, 1982).

[19] J. Guckenheimer and P. Holmes, Nonlinear Oscillations, Dynamical Systems and Bifurcations of Vector Fields (Springer, New York, 1983).

[20] M. Urabe and A. Reiter, Numerical computation of nonlinear forced oscillators by Galerkin's procedure, J. Math. Anal. Appl. 14 (1966) 107–140.

[21] M. Urabe, Nonlinear Autonomous Oscillations (Academic Press, New York, 1967).

[22] E. Brommundt, On the numerical investigation of nonlinear periodic rotor vibrations, in: Dynamics of Rotors, IUTAM-Symposium in Lyngby, Denmark (Springer, Berlin, 1975) 75–102.

[23] E. Brommundt, Bifurcation of self-excited rotor vibrations, in: Proc. Internat. Conf. Non-Linear Vibrations (Akademie-Verlag, Berlin, 1977) 123–134.

[24] R. Seydel, From Equilibrium to Chaos. Practical Bifurcation and Stability Analysis (Elsevier, New York, 1988).

[25] J. Awrejcewicz, Gradual and sudden transition to chaos in a sinusoidally driven oscillator, J. Phys. Soc. Jap. 58 (1989) 4261–4264.

[26] J. Awrejcewicz, Three routes to chaos in simple sinusoidally driven oscillators, J. Appl. Math. Mech. (Z. Angew. Math. Mech.) 70 (10) (1990) 1–9.

[27] J. Awrejcewicz, Numerical investigation of periodic motions of the human vocal cords including stability and bifurcation phenomena, Dyn. Stab. Syst. J. 5 (1) (1990) 11–28.

[28] J. Awrejcewicz, Bifurcation portrait of the oscillations of the human vocal cords, J. Sound Vibration 136 (1) (1990) 151–156.

[29] J. Awrejcewicz, Vibration system: Rotor with self-excited support, in: Proc. Internat. Conf. on Rotordyn., Tokyo (14–17 September 1986) 517–522.

[30] J.M.T. Thompson and H.B. Stewart, Nonlinear Dynamics and Chaos (Wiley, Chichester, 1986).

[31] G. Hall and J.M. Watt, Modern Numerical Methods for Ordinary Differential Equations (Clarendon Press, Oxford, 1976).

[32] V.I. Arnold, Geometrical Methods in the Theory of Ordinary Differential Equations (Springer, New York, 1983).

[33] J.I. Neimark, Dynamical Systems and Control Processes (Nauka, Moscow, 1978) in Russian.